Development of the technical capabilities needed to build and position a prepolarization coil for a magnetic resonance imaging magnet

M Jaensch, I R Young, C Besant, A Atkins, and **M Lamperth***
Department of Mechanical Engineering, Imperial College, London, UK

The manuscript was received on 17 October 2005 and was accepted after revision for publication on 25 September 2006.

DOI: 10.1243/09544119JEIM114

Abstract: An experiment to show that a magnetic resonance imaging (MRI) magnet could be assembled around a patient, and used as part of a prepolarization system in which substantial transient forces are applied to parts of it, is described. The paper describes the circumstances that develop as a result of the application of the large transient fields used in this type of study, and outlines the reason for the tolerances that are permissible on the alignment of the system components. It then describes a test rig used to evaluate how the various problems might be overcome, and reports on the performance achieved with this rig. On the basis of this work, it appears that a system could be developed that would allow the application of these methods in clinical MRI.

Keywords: MRI, prepolarization, precise position control, vibration attenuation

1 INTRODUCTION

Nuclear magnetic resonance (NMR) theory predicts an increasing signal-to-noise ratio as the main magnetic field used is increased [**1**]. The increase in performance with field in magnetic resonance imaging (MRI) is less than that found with conventional high-resolution MRI (as the body, which constitutes the load on the coils detecting the signal, is conducting) but is still substantial [**2**], and this is the fundamental reason for the use of cylindrical cryogenic magnets, which can easily be designed to operate at high fields, as the core of clinical and other MRI systems [**3**].

However, such magnets are difficult to use in many circumstances, particularly where an interventional procedure is required, and many patients find them unacceptably claustrophobic. Open magnets of various types have been developed, but all of them tend to have lower field levels than the solenoidal configuration [**4**]. Typical designs include iron-yoked 'C' magnets which allow good access to the patient from the side and are comforting as the patient can practically always look sideways out of the magnet.

One compromise, which allows some of the advantages of the higher field while allowing the better patient access afforded by the lower field units, is the use of prepolarization. In this method, which is generally targeted at a limit fraction of the whole volume of the body in the machine, a coil arrangement is used to apply a large field for a limited period of time before it is removed and data recovery begins.

This strategy means that the field quality of the additional field can be very poor compared with the few parts per million (ppm) error which is all that is permissible during the data acquisition process. Unlike this latter stage, where signals at differing fields dephase each other extremely quickly and useful data soon become unrecoverable, the effects of field inhomogeneity during the application of the high field result in a signal amplitude variation. This is normally tolerable, and a correction can easily be made if the coil configuration is known. Various approaches to prepolarization are possible, but the version investigated here is the simplest and most direct. In this, a current pulse of appropriate duration is fed to a coil (or pair of coils) adjacent to the region from which an enhanced signal is desired.

** Corresponding author: Department of Mechanical Engineering, Imperial College, Exhibition Road, London SW7 2AZ, UK. email: m.lamperth@imperial.ac.uk*

The present paper begins with a brief analysis of the form of prepolarization investigated, in order to demonstrate the key engineering features of the method that have to be resolved before it can be applied in practice. Thereafter, the experiment performed to demonstrate how the method could be implemented in practice is described, and the results obtained from the test rig employed are presented, before considering what other problems have to be overcome before the system can be used in clinical practice.

2 PREPOLARIZATION

The principal requirement for an MRI study is a large volume of highly homogeneous magnetic field (typically with deviations of no more than 5–10 ppm about the mean). The direction of this field is conventionally taken as the Z axis of a three-dimensional frame of reference. Nuclei capable of being involved in NMR experiments align along it, with a very small preponderance in one direction (as determined by the Curie relationship [**5**], which relates the level of magnetization to the applied field.)

The main NMR field is conventionally designated as B_0, more exactly as a vector quantity $\boldsymbol{B}_0$. If a second field $\boldsymbol{B}_\mathrm{p}$, also a vector quantity, is added to the first field, the nuclei seek to align along the resultant $\boldsymbol{B}_0+\boldsymbol{B}_\mathrm{p}$ field. If $\boldsymbol{B}_\mathrm{p}$ is generated by a simple coil structure, such as a planar winding, it will vary both in amplitude and in orientation from place to place in the region near it. This is the sort of coil that might typically be used in prepolarizing equipment, although generally, and if practicable, there might be a second similar coil on the other side of the patient (in a clinical MRI system).

In practice, a coil like this is pulsed, partly because the transient power requirements it demands can be very significant (even if, as in the present work, the coil to be used is superconducting), and partly because the field has to be removed in order that the homogeneous field essential for data recovery can be achieved once more.

It has been determined in huge numbers of MRI studies that the key diagnostic features that have made the technique so powerful are derived from differences in the relaxation time constants between normal and abnormal tissues. There are two primary time constants [**6**] (known respectively as the longitudinal time constant, T_1, and the transverse time constant, T_2). The former is always greater than, or equal to, the latter, and can be enormously greater (as it is in most solid or quasi-solid systems). In typical tissues (both normal and abnormal, and ignoring tissues such as cortical bone), T_1 is typically 3–10 times T_2.

Prior to the application of the prepolarizing field, the magnetization of the tissue will be proportional to the magnetization Mxy_0; after the application of the prepolarizing field it will increase towards proportionality with $M_{xy_0}+M_{xy_\mathrm{p}}$ ($=\mathrm{M}_{xy_{\mathrm{a}0}}$, the ultimate field at a point A) with time constant T_1. If t_p is the time that has elapsed since the application of the prepolarizing field (which is assumed to be a square pulse), then

$$M_{xy_{\mathrm{at}}}=M_{xy_0}+M_{xy_\mathrm{p}}[1-\exp(-t_\mathrm{p}/T_1)] \tag{1}$$

Note that this relationship assumes that a very long time has occurred since the system was last interrogated, so that the magnetization Mxy_0 alone has had time to recover completely. As will be seen below, if this is not so, there is an additional complication.

Once the prepolarizing pulse has been removed, the system has to recover to its state prior to the application of the pulse. Since, as can be seen in equation (2), the magnetization enhancement, which has been achieved at once, starts to decay to its steady state (Mxy_0) value, it is vital that the recovery time t_s be minimized. In practice, the speed at which the current in the prepolarizing coil can be reduced is determined by the technology used in its design, and, in this instance, using a superconducting coil, the time taken is around 50 ms, although alternative designs might allow much shorter intervals. The recovery time t_s is in practice the sum of the time needed to remove the field and the period subsequent to that needed to stabilize the system sufficiently for NMR operations to begin.

The magnetization available at the end of time t_s at an arbitrary point A is then proportional to the residual magnetization $M_{xy_{\mathrm{ar}}}$, where

$$M_{xy_{\mathrm{ar}}}=M_{xy_0}+M_{xy_{\mathrm{pa}}}[1-\exp(-t_\mathrm{p}/T_1)]\exp(-t_\mathrm{s}/T_1) \tag{2}$$

The actual signal obtained is proportional to the actual proton density distribution and the time constants of the tissues at the site of the measurement. With additional subscripts to identify the parameters at point A, the available signal S_a from the small voxel of volume v surrounding it is then

$$S_\mathrm{a}=K\rho_\mathrm{a}v(M_{xy_0}+M_{xy_{\mathrm{pa}}}[1-\exp(-t_\mathrm{p}/T_{1\mathrm{a}})] \times\exp(-t_\mathrm{s}/T_1)[1-\exp(-T_\mathrm{R}/T_{1\mathrm{a}})]\exp(-T_\mathrm{E}/T_{2\mathrm{a}}) \tag{3}$$

where K is a proportionality constant relating actual magnetization to the output signal, and accommodating a number of fixed factors including the detector system geometry and the operating frequency of the machine; ρ_a is the density of the nuclei being observed (normally protons in clinical applications of MRI) at point A; T_R is the period since the centre of the last RF pulse exciting the spin population [noting that the formulation in equation (3) assumes that all the spins that are available to be excited have been, as otherwise additional terms are required in the relationship, and that the recovery of the magnetization from the previous excitation affects the amount available for prepolarization as well as for normal operation]; and T_E is the time between excitation of the spins prior to data collection and the time at which the centre of spatial–frequency (k-) space is acquired. This can be very short, but its effects are increased by the relatively short spin dephasing time (implicit in the relatively smaller T_2 times). The relationship must be modified to reflect the real structure of the prepolarizing pulse (for example, that used in the description that follows) and quickly becomes very complex.

As it has evolved, it has become apparent that much of the clinically useful information resides in the time constants, and much effort has gone into optimizing the strategies needed to maximize image contrast based on them [**7**, **8**]. It has also emerged that the time constants of tissue, among most other materials, are field dependent (although only the variations of T_1 are of importance in the range of fields used in clinical work [**9**]). Any of the times in the numerators of the various exponential terms are potential means of adjusting the signal overall, and, through the differences in the relaxation parameters between tissues, adjusting image contrast. In practice, only T_R and T_E are widely used for this purpose, although in a prepolarization experiment, particularly if the pulsed field is large compared with $\boldsymbol{B}_0$, variation of t_p is a very powerful tool.

Without attempting to explain the reasons for the detailed design of the operational procedure, since those depend on a description of the NMR requirements which extends very far beyond the scope of this paper, Fig. 1 and Table 1, with a supporting set of data, show the timing of the various necessary operations in a prepolarizing study in which the MRI data acquisition sequence used is a slice-selective gradient recalled echo (GRE – the current name for the original Aberdeen spin warp sequence [**10**]).

Figure 1 shows the sequence structure in outline, showing the data recovery part of the sequence as a block (which actually involves the operation of two gradients and a data acquisition system) for simplicity. As mentioned, practical constraints on the polarizing coil design meant that the ramp downtime had to be at the top end of the desired range, although the total duration of t_s is very slightly longer.

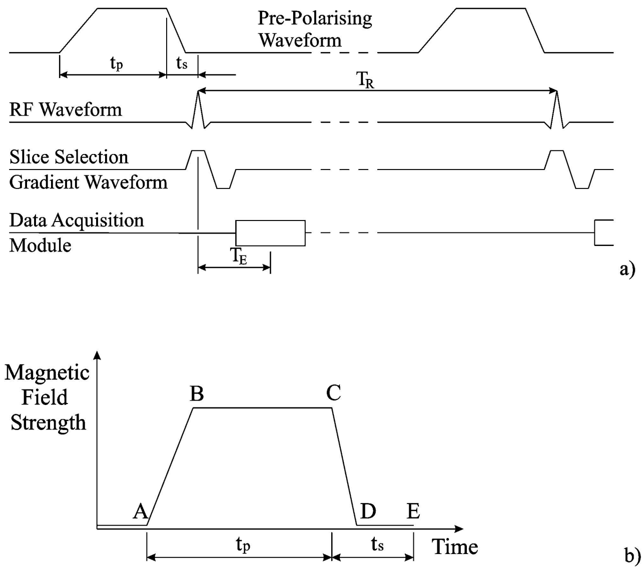

Fig. 1 (a) Overall sequence, in which the recovery time T_R is the longest period while T_E is the time between excitation and the time at which the centre of k-space is sampled. (b) Prepolarization pulse structure. While the pulse must be ramped down very fast, there are no similar constraints on the ramping-up, although the efficiency of the polarizing action suggests it should not be too long. Note that A to C comprise t_p, while C to E is t_s

Table 1 Typical range of practical polarizing pulse parameters

Sequence	Description	Duration (ms)
A–B	Prepolarizer ramped up	25–100
B–C	Polarizing time	50–500
C–D	Polarizer field ramped down	5–50
D–E	Recovery period	5–50 (max.)

This sequence is both the simplest and the most vulnerable to any field disturbance. It is designed to be capable of substantial T_1 weighting, which is consistent with the point made above about the use of the duration of the prepolarizing pulse to affect the contrast of the images through the dependence of the achieved magnetization on T_1.

3 PREPOLARIZER PERFORMANCE REQUIREMENTS

Examination of equation (3) indicates which of the various parameters are most important in a prepolarization system, and suggests the major factors that have to be addressed in making such a system work. It is easiest to start with the situation immediately prior to the beginning of the prepolarization pulse, and compare that with the situation that must exist when data acquisition commences. A working rule of thumb (J. V. McGinley, 2000, personal communication) is that a mechanical displacement of any coil or iron component of a magnet of 1 μm results in a field change of about 1 ppm. High-quality imaging magnets are normally specified by the size of their imaging volume at a particular quality of field – very typically ± 5 ppm.

Any structure carrying a prepolarizing system will be designed to include relatively little iron, because it will remain in position during data acquisition (after the field pulse has been removed) and any movement is undesirable. However, because the structure will be arranged to be very close to the patient, it can be conveniently used to support other parts of the MRI and the magnet shimming system. (All magnets, however good their design and manufacture, require additional coils or more usually iron pieces, which must be very accurately placed and adjusted in order to achieve their final specifications.)

The specification for the recovery of the prepolarizer to its prepulse position, over an indefinite number of pulse cycles at 1 s intervals, was ± 2 μm in any direction with a maximum angular error of 2 arcsec. As equations (2) and (3) indicate, it is essential that t_s be kept as short as possible in order that the additional magnetization that has been created does not just decay away before it can be exploited. Since most tissue T_1 values lie in the range 150–1000 ms at the fields of most concern, it is important that t_s be kept less than 50 ms. (This still means a loss of nearly 30 per cent of the gain in magnetization for the shortest component tissues. However, these comprise mainly fatty materials that are generally of less significance from a clinical point of view.)

It must be borne in mind that, during the application of the prepolarizing pulse, the field generated by it will cause major forces to be applied both to the prepolarizing system and to the magnet generating $\boldsymbol{B}_0$. The force applied to the test rig, based on the system being installed in a 0.2 T resistive magnet and generating a prepolarizing field of 0.15 T at 100 mm from the coil surface, was specified as 1.367 kN. The control of the consequences of this force was the basis of the study described in the next sections of this paper.

One final – and vital – factor is that any system that is installed must avoid introducing any artefacts into the MRI data that are being obtained. This means that the control system must be as free of ferromagnetic components as possible, and that any RF noise introduced by the control system must be sufficiently far (at least 1 MHz) and well attenuated by filters from the resonant frequencies of any nuclei that might be targeted in the machine (although, in practice, the proton resonance is the only significant one).

4 DESCRIPTION OF THE TEST RIG

The open MRI scanner with which it was proposed the prepolarizer might be used has a C-type iron-yoked magnet operating at 0.2 T (Siemens, Erlangen, Open). The prepolarizing system was planned to be moved back from the magnet and then inserted into the system above the patient for imaging. For investigational purposes, it was decided to use a cantilever structure to support the prepolarizing magnet, with the arm carrying it being allowed to rotate through 100° about its support column. The concrete-filled column was securely bolted to the floor and the arm allowed to rotate about the top of the column on a bearing system based on four high-precision angular contact bearings located within the column.

The arm and column were designed to be of maximum stiffness in order to increase the repositioning accuracy and reduce the effect of vibrational forces occurring owing to the ramping down of the prepolarizer coil current. The arm was manufactured out of type 316 stainless steel to achieve a good compromise between MR compatibility on the one hand and cost, strength, and ease of manufacture on the other. Aluminium, which is well known to be MR compatible [**11**], was used for the coil chassis containing the prepolarizing magnet.

Figure 2 shows the prepolarizer support structure as assembled in the laboratory at Imperial College. The structure placed on the left of the arm is an

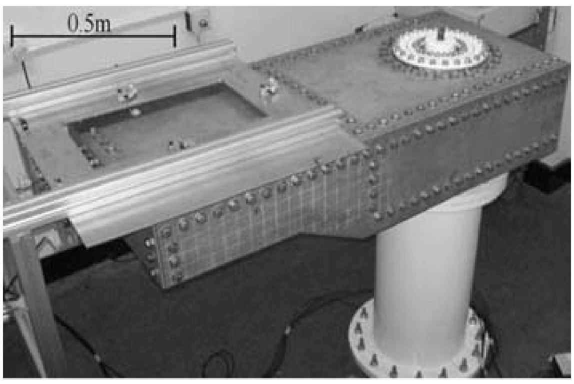

Fig. 2 Prepolariser support structure

aluminium frame used as a reference for measuring the position of the prepolarizing coil. For further investigations, this reference frame can be replaced with the actual C-type background magnet (see Fig. 3).

As neither the required accuracy of repositioning the prepolarizing coil after having been moved out of and back into the imaging position nor the stabilization of the coil during imaging could be provided by the passive structure alone, an active positioning and vibration attenuation system was developed and integrated into the coil support structure.

While conventional vibration attenuation systems often rely on velocity feedback using accelerometers [**12**, **13**], this system utilizes integrated position feedback provided by optical fibre sensors (Philtec D20) in combination with an FPGA-based PID controller (National Instruments PXI-7831R) and piezoelectric actuators (Physikinstrumente P-844.20 and P-844.30). Piezoelectric actuators are widely used for micropositioning applications due to their submicrometre accuracy [**14**]. The ability to generate high forces as well as a fast response time also makes them suitable for micrometre vibration attenuation [**15**]. Preliminary investigations showed that the performance of the active system is not affected by the presence of a magnetic field.

The prepolarizing coil was mounted in an aluminium chassis, which was attached to the arm by three vertically and three horizontally mounted piezoelectric actuators, thus providing active control in six degrees of freedom (DOF). Figure 4 shows how the aluminium coil chassis was suspended in the arm.

Utilizing Ansys 8.0, the finite element (FE) model depicted in Fig. 5 was built up to aid the design process and allow predictions concerning the mechanical properties and the vibration behaviour of the

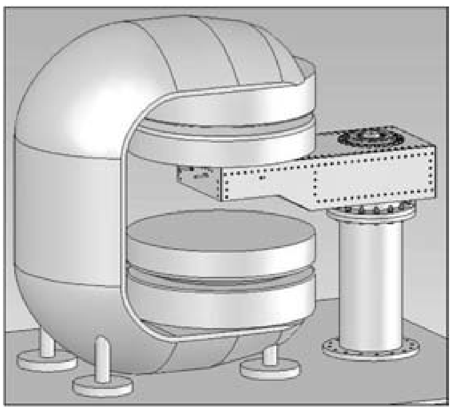

Fig. 3 Prepolariser support structure and background magnet

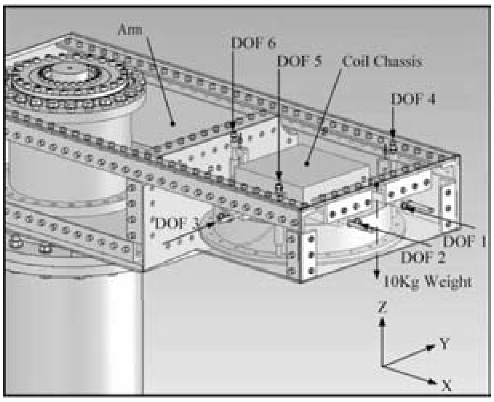

Fig. 4 Suspension of the coil chassis

Fig. 5 FE model of the prepolariser support structure

support structure. In the frequency domain the FE model of the structure was validated against the actual structure using modal analysis techniques. The data collected from an experimental modal analysis were compared with the data obtained from a modal analysis carried out using the FE model. The results are presented in Table 2, where the first five modes of vibration are identified together with their respective natural frequencies.

In the time domain, however, the following test was made to demonstrate the ability of the FE model accurately to predict the dynamic behaviour. A 10 kg mass was hung by a thread attached to the tip of the beam, as indicated in Fig. 4. After cutting the thread and thus releasing the weight, the beam moved

Table 2 Comparison of measured and predicted resonant modes

Mode number	Frequency of measurement (Hz)	Frequency of prediction (Hz)	Description
1	50	51.5	First x bending
2	53.5	52.5	First y bending
3	87	87	First coil rotation
4	105	104	Second y bending
5	139	140	Second coil rotation

freely. The transient behaviour of the arm was measured by one of the vertical displacement sensors – DOF 4 in Fig. 4 – over the first 25 ms period, and this was compared with the transient response predicted. The results are shown in Fig. 6, where it can be seen that the FE model predicts the transient behaviour to within 0.7 μm over the 25 ms period.

An additional finite element analysis of the C-type background magnet, which was originally supposed to be part of the experimental set-up, determined that the corresponding pulsatile force on the background magnet, exerted by the prepolarizing coil, would cause it to vibrate. The instability that was found was such that it would not be possible to image with the prepolarizer in that particular design of magnet, although a different but entirely practical magnet design would make this possible.

5 RESULTS FROM THE TEST RIG

A series of tests were performed on the test rig to determine if it would position and stabilize the prepolarizing coil within the specification under operating conditions.

5.1 Accuracy of positional repeatability

The positional accuracy of the coil assembly was measured with the arm being moved into and away from the imaging position. The following sequence was performed 50 times:

(a) measurement of the position of the coil chassis in all six DOF;
(b) unlocking the end stops;
(c) moving the arm out of the imaging position by around 90°;
(d) returning the arm back into the imaging position;

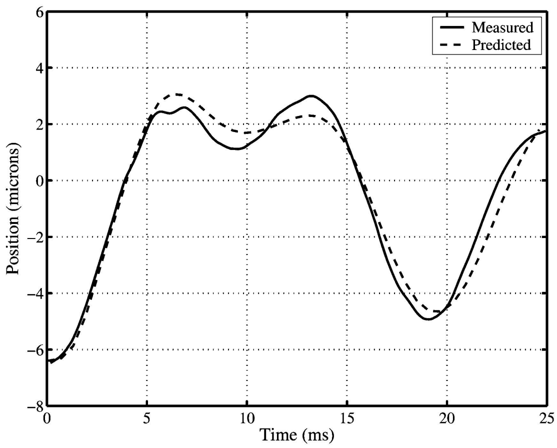

Fig. 6 Measured and predicted response of the arm

(e) locking the end stops;
(f) measurement of the position of the coil chassis in all six DOF.

The data from the measurements showed that there was a very small but cumulative error each time the arm was moved. The mean error, m, together with the standard deviation, s, was determined for each DOF. The relocation error, e, was then determined from

$$e = m + 3s \qquad (4)$$

The results for the six DOF are given in Table 3.

It can be seen from the results that the arm is sufficiently rigid to ensure that the coil can be passively relocated within the given margin in four out of the six DOF. The active position control system makes it possible to position the coil chassis in all six DOF with an accuracy of less than ± 0.5 μm. This limit is given by noise originating in the optical position sensors. Thus, using the active positioning system, the coil chassis can easily be repositioned to within the required accuracy. A positional accuracy of less than ± 0.5 μm for all six actuator/sensor pairs is equivalent to a positional accuracy of the coil of less than ± 0.5 μm in each direction and less than ± 1 arcsec for any rotation.

Calculations suggest that the cumulative error observed would exceed the maximum travel of the actuators after approximately 165 relocation exercises. However, further tests concerning the long-term stability showed that environment effects were apparent in the results. For example, DOF 1 was tracked over a period of several days, and in 1 h the sensor on DOF 1 had shown a movement of 5 μm. In a similar 1 h period, when up to 20 relocations had been made, the coil chassis was shown to have moved 4.5 μm. Thus, it can be concluded that environmental effects such as temperature changes were mainly responsible for the cumulative error, and the number of possible relocations is actually much higher. It should be noted that the room where the arm was located was not temperature controlled.

Table 3 Accuracy of repositioning of the test rig arm

Degree of freedom	Mean error, m (nm)	Standard deviation, s (nm)	Relocation error, e (nm)
DOF 1 (front)	185 ± 116	306	185 ± 1034
DOF 2 (front)	184 ± 110	291	184 ± 983
DOF 3 (side)	131 ± 682	1798	131 ± 5504
DOF 4 (vertical)	-42 ± 293	773	-42 ± 2612
DOF 5 (vertical)	-47 ± 208	548	-47 ± 1852
DOF 6 (vertical)	127 ± 171	452	127 ± 1527

5.2 Accuracy measurements under varying arm loading

It is of particular importance that the positional accuracy be maintained under transient arm loading conditions such as when the prepolarizer coil current is ramping down. The finite element model was used to predict the transient behaviour before and during the imaging process. For this analysis, a force profile indicating the transient removal of the magnetic force on the prepolarizer coil was calculated using three-dimensional finite element analysis (vector field). Figure 7 shows the predicted relation between the magnetic field intensity ($\mathbf{B}_0 + \mathbf{B}_\mathrm{p}$) and the force acting on the prepolarizer coil when ramping down the prepolarizer coil current.

The calculated movement of the coil chassis in each direction in the first 75 ms after ramping down commenced is depicted in Fig. 8.

An expanded view of the crucial time at which it is desirable that imaging starts is given in Fig. 9.

The analysis of the movements of the coil chassis in the various DOF shows that movements in the vertical z direction were the most critical, with oscillations of ± 4 µm. To simulate the vibration of the manipulator before imaging commences, and to demonstrate the effectiveness of the active vibration attenuation system, the following test was devised.

The arm was loaded at its end with a 10 kg mass that was suspended on a thin wire attached to the front end of the beam, as indicated in Fig. 4. When the wire was cut, the coil chassis suspended in the arm started to vibrate. Choosing a weight of 10 kg provokes oscillations, which are 25 per cent higher than those occurring in the crucial phase just before imaging commences. Thus, the vibration attenuation system could be tested under worst-case conditions. Two tests were performed with the active vibration control turned off and on. The results are shown in Fig. 10.

The maximum deviation in position of the coil chassis after release is 5.2 µm with active control and 1.2 µm without active control. This is equivalent to

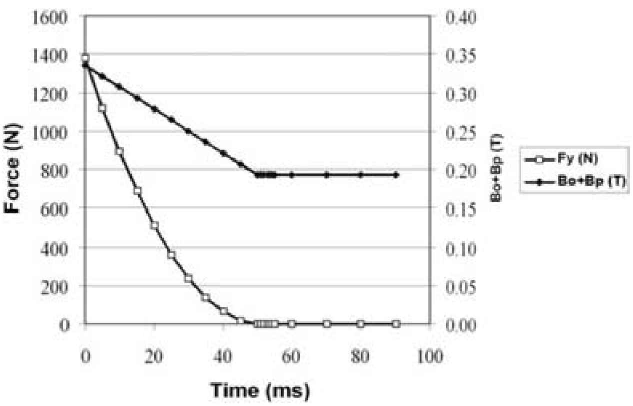

Fig. 7 Magnetic field density and force on the coil during ramping down

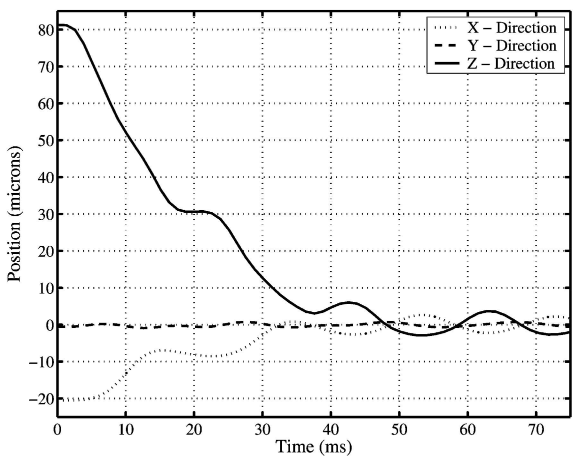

Fig. 8 Calculated movement of the coil chassis

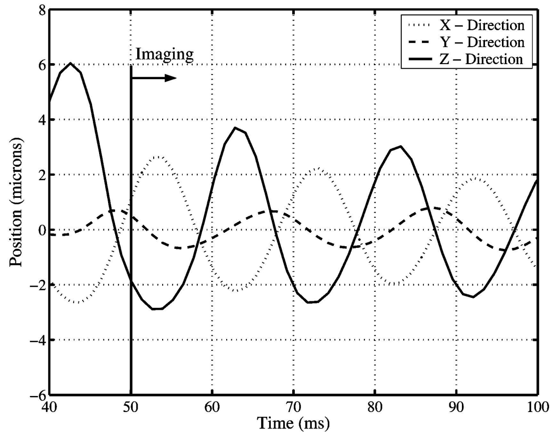

Fig. 9 Calculated movement of the coil chassis (expanded view)

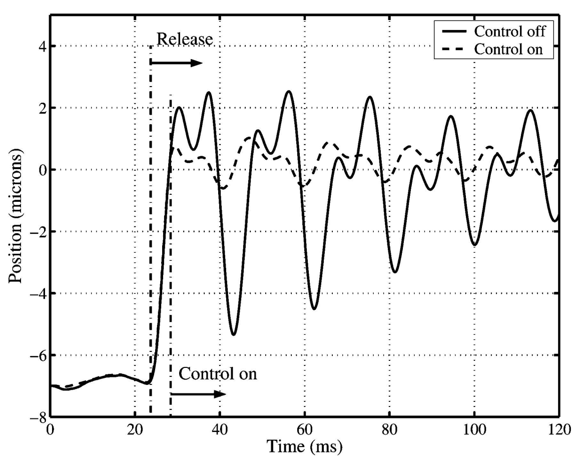

Fig. 10 Measured movement of the coil chassis with and without active control

Table 4 Maximum amplitude of motion during imaging with active control

Type of oscillation	Maximum amplitude	Limit
Movement in x direction (μm)	2.5	2
Movement in y direction (μm)	0.8	2
Movement in z direction (μm)	0.9	2
Rotation about x axis (arcsec)	0.2	2
Rotation about y axis (arcsec)	0.8	2
Rotation about z axis (arcsec)	0.3	2

a reduction of -13 dB. Thus, utilizing the active vibration and position control system under actual operating conditions, the maximum vertical movement of the coil during imaging can be reduced from ± 4 μm to ± 0.9 μm. Furthermore, it can be seen that the control system works immediately and without overshooting once activated.

The maximum amplitudes of motion of the prepolarizing magnet during the imaging phase in translational as well as rotational terms, as compiled in Table 4, are derived by analysing Fig. 9 and taking into account the discussed vibration-attenuating effect of the active vibration control system.

However, the active control system not only reduces the amplitude of motion of the coil during imaging but also stabilizes the coil against impulse loading. Figure 11 shows the response of the structure, as measured by one of the vertical displacement sensors, when the beam was subjected to several vertical impacts by collision with a small hammer.

6 DISCUSSION

None of the standard imaging magnets to which access would have been possible for trials of the system in the mode for which it was originally designed were stable enough themselves not to react to the pulsed forces that would have been applied to them. The authors were thus unable to demonstrate the performance of the system in the environment for which it is intended. Some preliminary work to evaluate the response of a typical iron-yoked MRI electromagnet, involving both finite element analysis and direct measurements, made this very clear. On the other hand it is not unreasonable that a magnet designed to operate in one particular manner can perform adequately in a totally different way. What it is believed this preliminary work has shown is that, if operating in pulsed prepolarizing mode were to be specified, it would be possible to design a system that could do so.

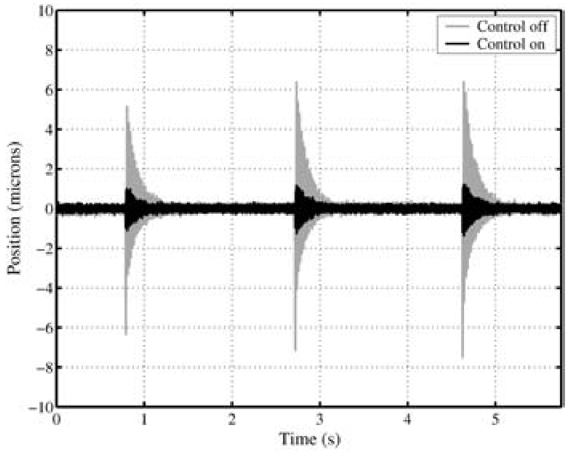

Fig. 11 Effect of impulse loading on the arm with and without active control

The performance of the test rig demonstrates that the necessary stabilities and reproducibilities can be achieved. The test in which the cutting free of the load was used to simulate the pulsed load imposed by the operation of the prepolarizer coil is arguably not truly representative of the actual conditions that will exist in a real system, but it does adequately model the transient conditions that will exist only a very few milliseconds after the prepolarizer pulse has been removed. The stability test described in the first part of the review of the rig performance is, in some ways, of less importance in prepolarization than the transient response, but it is very significant in other respects, as the following will make clear.

Although the experimental work described was all directed at prepolarization, it does have a much broader potential. Magnets are very awkward and large, and it is hard for clinicians to gain the sort of access to patients they need to perform many interventional procedures. Patients, attached as they frequently are to numerous drip and monitoring lines, can only be moved with difficulty, and with the perpetual risk that something may be dislodged in the process. Moving the magnet to the patient is an expedient that has been investigated [**16**], and has shown some promise, although very few examples of this have been produced. Another possibility is the assembly of the magnet around the patient during the operation or other procedure. It should be noted that imaging is usually required during only a very small fraction of the time the patient is on the operating table, so that moving parts of the magnet structure into place when needed and keeping them out of the way for the rest of the time is a potentially very useful capability. The specifications for assembling a magnet in this way, and the problems likely to be encountered in doing this, are very similar to those used in this study, and the repeatability test described in the previous section gives great confidence that magnets can indeed be assembled in any way that might be needed. It would be possible, for example, on the basis of the work described here, to use the same techniques and methods to bring in the upper section of a yoked magnet to align with the lower part, although the weights and dimensions involved would be rather greater.

7 CONCLUSIONS

The feasibility of designing and making a system in which large transient fields could be applied during an MRI study and then removed prior to the acquisition in such a way that the majority of the gain generated by the pulsed field could be exploited has been demonstrated. Further, this work lends credence to the idea that it will be possible in future to develop and manufacture whole-body MRI systems in which the magnet can be split to allow better access to the patient at various stages of an operation or other interventional procedure, with the magnet being reassembled around the patient when imaging is required.

In particular, it has been shown that it is possible to build a support structure that allows the prepolarizing coil to be moved in and out of the background magnet with the accuracy required for MR imaging. Using an active position control system, the achievable accuracy in repositioning was found to be less than $\pm 0.5\,\mu$m in each direction and less than ± 1 arcsec for any rotation. A thoroughly validated finite element model was utilized to predict the movements of the coil chassis before the imaging phase. Tests showed that the newly developed active vibration attenuation system can reduce the oscillation of the coil chassis during the imaging period to within the given limits of ± 2 μm in each direction and ± 2 arcsec for any direction.

While the active position control system implemented in the current configuration can cope with any short-term effect, such as the deviation in position after relocating the coil chassis, it might be necessary to add a second positioning system to cope with long-term effects caused by environmental influences and the repeated loading during imaging. These effects cause a deviation of the coil chassis from its original position, which eventually might exceed the maximum travel provided by the piezoelectric actuators and thus result in improper positioning.

ACKNOWLEDGEMENTS

The work described was funded by the Department of Health through MedLINK project grant 217 (EPSRC GR/R73812/01) and was a combined project between the Department of Mechanical Engineering at Imperial College, London, and Siemens Magnet Technology, Eynsham, Oxford. The rig programme was implemented at Imperial College while the HTSC superconducting coil was designed and built by Siemens Corporate Technology PS3, Erlangen.

REFERENCES

1 **Hoult, D. I.** and **Richards, R. E.** The signal-to-noise ratio of the nuclear magnetic resonance experiment. *J. Magn. Reson.*, 1976, **24**, 71–85.
2 **Hoult, D. I.** and **Lauterbur, P. C.** The sensitivity of the zeugmatographic experiment involving human samples. *J. Magn. Reson.*, 1979, **34**, 425–433.
3 **Rayner, D. L., Feenan, P. J.,** and **Warner, R. J.** Cryogenic magnets for whole body magnetic resonance systems. In *Methods in biomedical magnetic resonance and spectroscopy* (Ed. I. R. Young), 2000, pp. 109–114 (Wiley, Chichester).
4 **Davies, F.** Resistive and permanent magnets for whole body MRI. In *Methods in biomedical magnetic resonance and spectroscopy* (Ed. I. R. Young), 2000, pp. 103–109 (Wiley, Chichester).
5 **Abragam, A.** *Principles of nuclear magnetism*, 1961, pp. 1–4 (Oxford University Press, Oxford).
6 **Abragam, A.** *Principles of nuclear magnetism*, 1961, pp. 19–22 (Oxford University Press, Oxford).
7 **Bydder, G. M.** The advance of NMR. *Lancet*, 1984, **I**, 21–23.
8 **Young, I. R., Burl, M.,** and **Bydder, G. M.** Comparative efficiency of different pulse sequences in NMR imaging. *J. Comput. Assist. Tomogr.*, 1986, **10**, 271–286.
9 **Bottomley, P. A., Foster, T. H., Argersinger, R. E.,** and **Pfeifer, L. M.** A review of normal tissue hydrogen NMR relaxation times and relaxation mechanisms from 1–100 MHz. Dependence on tissue type. *Med. Physics*, 1984, **11**, 425.
10 **Hutchison, J. M. S., Edelstein, W. A.,** and **Johnson, E.** A whole body NMR imaging machine. *J. Physics E., Sci. Instrum.*, 1980, **13**, 947–955.
11 **Chinzei, K., Kinkines, R.,** and **Jolesz, F. A.** MR compatibility of mechatronic devices: design criteria. In Proceedings of Second International Conference on Medical Image Computing and Computer-Assisted Interventions, Cambridge, UK, 1999, Lecture Notes in Computer Science, pp. 1020–1031.
12 **Huang, X., Elliot, S. J.,** and **Brennan, M. J.** Active isolation of a flexible structure from base vibration. *J. Sound and Vibr.*, 2003, **263**, 357–376.
13 **Preumont, A.** *Vibration control of active structures*

– *an introduction*, 2002, pp. 113–118 (Kluwer Academic Publishers, Dordrecht).

14 **Juhas, L., Vujani, A., Adamovic, N., Nagy, L.,** and **Borovac, B.** A platform for micropositioning based on piezo legs. *Mechatronics*, 2001, **11**, 869–897.

15 MicroPositioning, NanoPositioning, NanoAutomation, Physikinstrumente Products Catalogue, 2001.

16 **Hoult, D. I., Saunders, J. K., Sutherland, G. R., Sharp, J., Gervin, M., Kolansky, H. G., Kripiakevich, D. L., Procca, A., Sebastian, R. A., Dombay, A., Rayner, D. L., Roberts, F. A.,** and **Tomanek, B.** The engineering of an interventional MRI with a moveable 1.5 Tesla magnet, *J. Magn. Reson. Imaging*, 2001, **13**, 78–86.